UC Davis
UC Davis Previously Published Works

Title

Ion-Induced Defect Permeation of Lipid Membranes

Permalink

https://escholarship.org/uc/item/41n899jn

Journal

Biophysical Journal, 106(3)

ISSN

0006-3495

Authors

Vorobyov, Igor
Olson, Timothy E
Kim, Jung H
et al.

Publication Date

2014-02-01

DOI

10.1016/j.bpj.2013.12.027

Peer reviewed

Ion-Induced Defect Permeation of Lipid Membranes

Igor Vorobyov,[¶] Timothy E. Olson,[‡] Jung H. Kim,[‡] Roger E. Koeppe II,[§] Olaf S. Andersen,[‡*] and Toby W. Allen[†¶*]

[†]School of Applied Sciences and Health Innovations Research Institute, RMIT University, Melbourne, Victoria, Australia; [‡]Department of Physiology and Biophysics, Weill Cornell Medical College, New York, New York; [§]Department of Chemistry and Biochemistry, University of Arkansas, Fayetteville, Arkansas; and [¶]Department of Chemistry, University of California, Davis, Davis, California

ABSTRACT   We have explored the mechanisms of uncatalyzed membrane ion permeation using atomistic simulations and electrophysiological recordings. The solubility-diffusion mechanism of membrane charge transport has prevailed since the 1960s, despite inconsistencies in experimental observations and its lack of consideration for the flexible response of lipid bilayers. We show that direct lipid bilayer translocation of alkali metal cations, Cl^-, and a charged arginine side chain analog occurs via an ion-induced defect mechanism. Contrary to some previous suggestions, the arginine analog experiences a large free-energy barrier, very similar to those for Na^+, K^+, and Cl^-. Our simulations reveal that membrane perturbations, due to the movement of an ion, are central for explaining the permeation process, leading to both free-energy and diffusion-coefficient profiles that show little dependence on ion chemistry and charge, despite wide-ranging hydration energies and the membrane's dipole potential. The results yield membrane permeabilities that are in semiquantitative agreement with experiments in terms of both magnitude and selectivity. We conclude that ion-induced defect-mediated permeation may compete with transient pores as the dominant mechanism of uncatalyzed ion permeation, providing new understanding for the actions of a range of membrane-active peptides and proteins.

INTRODUCTION

The self-association of lipids into sheetlike bilayer structures, where lipid hydrocarbon tails are segregated from the aqueous phase, is a universal feature of cellular organization. Although the majority of charge transport across lipid membranes is regulated by specific channels and transporters, uncatalyzed ion permeation across membranes continues to be of much interest (1–3) and is important for understanding the movement and localization of charged amino acid side chains within membranes. This process is relevant to an expansive range of biological phenomena, including protein structure and function (see, e.g., Armstrong and Bezanilla (4) and Schmidt et al. (5)) and the actions of cell-perturbing peptides (e.g. ion channels; Melikov and Chernomordik (6) and Zasloff (7)), and has been shrouded in controversy after the publication of studies that challenged our understanding of membranes as barriers to charge movement (8–10). Here we have used molecular dynamics (MD) simulations and electrophysiological measurements to better understand and quantify charge-membrane transport processes.

A biological membrane is usually pictured as a bilayer of lipid molecules that form a low dielectric hydrocarbon sheet, where an ion must dehydrate to translocate (Fig. 1 A). Using this solubility-diffusion model, energy barriers for the movement of alkali metal and halide ions are far too high to be compatible with the observed permeability coefficients in membranes of typical thickness (1,11). Moreover, because solubility-diffusion energetics depend critically on hydration energy, this model yields highly selective permeabilities (assuming complete ion dehydration), varying by >10 orders of magnitude (12), contrary to existing experimental observations (13–15). Consequently, it has been assumed that unassisted ion permeation rather might occur via a transient pore mechanism (Fig. 1 B) (16), where local membrane defects create transmembrane pores that allow for nonselective ion permeation, in semiquantitative agreement with experiments (17).

Though the shortcomings of the solubility-diffusion model were recognized more than 40 years ago (18), it has remained the standard description of charge-membrane interactions. Recent MD simulations similarly have shown that a liquid-crystalline lipid bilayer perturbs significantly due to the fields of an ion, with water and lipid headgroups being pulled into the nonpolar core (19–23). In this description, which we refer to as an ion-induced defect mechanism, translocation occurs without the ion ever partitioning from water to hydrocarbon. Rather, the ion reshapes the interface as it moves (24) (Fig.1 C), causing a local membrane deformation that lowers the ion's energy without forming a complete hydrophilic pore for passive ion diffusion (Fig.1 B). Consequently, the energetics of permeation are different from those of a solubility-diffusion process in that they are primarily determined by the costs of membrane deformation as opposed to ion-dependent hydration energetics (21,25). Moreover, this deformation means that the ion does not cross the water-lipid interface to sense the full (strongly anion-selective (26–28)) dipole potential of the membrane (24). In addition to these molecular processes being fundamentally distinct, the energy barriers for ion-induced-defect-driven permeation are lower than those for solubility-diffusion by many kcal/mol (within bilayers

A *Solubility-diffusion*   **B** *Transient pore*
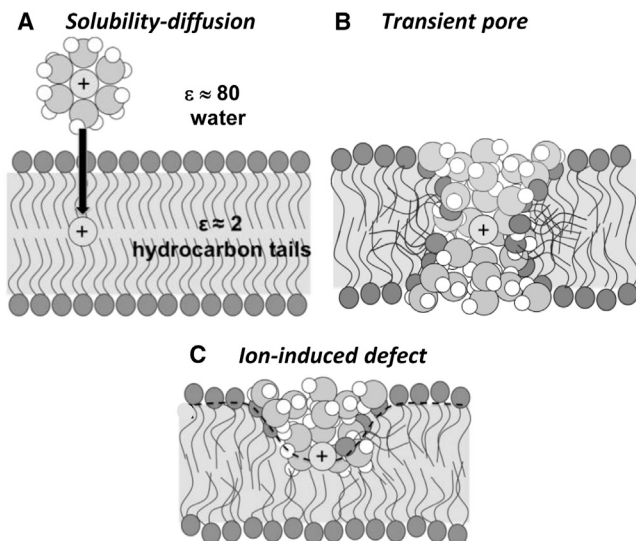

C *Ion-induced defect*

FIGURE 1   Possible mechanisms of ion permeation across lipid membranes.

below a critical hydrophobic thickness of ~32 Å (29)) and be within a regime that appears to be compatible with experimental measurements.

We therefore explored the permeation mechanisms, energetics, and permeabilities of different hydrophilic ions crossing lipid bilayers using MD simulation, and compared the predictions based on these simulations to new electrophysiological measurements. We can thus ascertain whether or not ion-induced-defect-driven permeation is consistent with experiment and whether it may compete with transient pores as a dominant conduction mechanism. In the process, we provide improved understanding of charge-membrane interactions relevant to a wide range of membrane proteins, toxins, antimicrobial and viral peptides.

MATERIALS AND METHODS

Fully atomistic simulations

MD simulations were carried out to study the permeation of the arginine side chain analog guanidinium (GuanH$^+$), and the physiological cations and anions, K$^+$, Na$^+$, and Cl$^-$, across a hydrated 1,2-dipalmitoyl-*sn*-glycero-3-phosphocholine (DPPC) bilayer. For direct comparison to experiments, we also simulated GuanH$^+$ crossing a branched 1,2-diphytanoyl-*sn*-glycero-3-phosphocholine (DPhPC) bilayer known to exhibit similar thickness and solubilities for a range of solutes and water (30,31). All simulations were done with CHARMM (32), using the C27 lipid force field (33) and TIP3P water (34) at 330 K (above the DPPC phase transition at ~314 K (35)). Bilayers were bathed in ~0.5 M aqueous KCl solution using ~45 water molecules/lipid. The potential of mean force (PMF), $W(z)$, for ion translocation was calculated via umbrella sampling (US) (36) and the weighted histogram analysis method (37), using 62 simulations of up to 16 ns each (for PMF convergence, see Additional simulation methods and Fig. S1 in the Supporting Material).

Spatially resolved diffusion coefficient profiles, D_z, were obtained by combining analysis of US simulations using the position autocorrelation function (38), mean-square displacement (MSD) analysis for a series of 2 Å slabs spanning interfaces and bulk, and true bulk estimates (D_{Bulk}) from separate electrolyte systems (see Ion diffusion calculation methods in the Supporting Material and Fig. S2). Permeability coefficients for each ion, P_{ion}, were calculated using an inhomogeneous solubility-diffusion model (39),

$$P_{\text{ion}} = \frac{K_{\text{ion}} \times D_{\text{eff,ion}}}{L}, \tag{1}$$

where L is the bilayer thickness, K_{ion} is the equilibrium partition coefficient into the bilayer (40),

$$K_{\text{ion}} = \frac{1}{L} \int_{-L/2}^{L/2} \exp(-W(z)/k_B T)\mathrm{d}z, \tag{2}$$

where k_B is Boltzmann's constant and T is temperature, and $D_{\text{eff,ion}}$ is the effective ion diffusion coefficient within the membrane (41),

$$D_{\text{eff,ion}} = \left(\frac{1}{L} \int_{-L/2}^{L/2} \exp(-W(z)/k_B T)\mathrm{d}z \right)^{-1} \\ \times \left(\frac{1}{L} \int_{-L/2}^{L/2} \frac{\exp(W_z/k_B T)}{D(z)}\mathrm{d}z \right)^{-1} \tag{3}$$

such that the calculated ion permeability is given by

$$P_{\text{ion,calc}} = \left(\int_{-L/2}^{L/2} \frac{\exp(W_z/k_B T)}{D(z)}\mathrm{d}z \right)^{-1}, \tag{4}$$

an integral over the local bilayer resistance (39). In all our calculations, this integral spans the range $-15 \leq z \leq 15$ Å, where the density of other ions vanishes, which is essential for modeling permeation by a single ion PMF (41). This description assumes that we are in the diffusion limit, where the mean velocity is proportional to the mean force, which is valid because the ion correlation length is short (~0.5 Å for Na$^+$; see Fig. S3 C) compared to the spatial variations in the force (39).

For comparison with experiments, we also calculated contributions to the membrane conductance, G_m, for each ion, $G_{\text{ion,calc}}$, related to $P_{\text{ion,calc}}$ via Eq. 7, to give (26)

$$G_{\text{ion,calc}} = t_{\text{ion}}G_m = \frac{N_A C q^2}{k_B T} P_{\text{ion,calc}}, \tag{5}$$

where t_{ion} is the ion transference number, defined below (Eq. 6), N_A is Avogadro's number, q is the ionic charge, and C is the salt concentration.

To investigate the penetration of ions into lipid bilayers at equilibrium, additional unbiased MD (uMD) simulations of DPhPC lipid bilayers solvated in 0.1 M or 1.0 M aqueous GuanHCl solutions were run at 330 K and 1 atm pressure for ~1.2 μs each, with the last 1.0 μs used for analysis. Simulation preparation and protocols for unbiased simulations are described in the Supporting Material. In graphs with error bars, the results depict mean ± standard error of mean (SEM).

Electrophysiology

Membrane currents were measured in symmetrical, unbuffered 0.1 or 1.0 M salt, using bilayer-forming solutions of DPhPC (which forms very stable,

high-resistance bilayers (42)) or ether analog, DphPC (to explore the role of dipole potential (28)) in n-decane or squalene. Reversal potentials (V_{rev}) were measured at 25°C using asymmetrical 0.1/0.2 M salt solutions. Experimental details are described in the Supporting Material. Transference numbers, t_{ion}, for cation and anion (t_+ and t_-) were determined from reversal potentials, V_{rev}, via (43)

$$t_+ = \frac{1 + V_{rev}/E}{2} \text{ and } t_- = 1 - t_+, \quad (6)$$

where E is the Nernst potential for the cation, allowing calculation of single-ion permeability coefficients (44),

$$P_{ion} = t_{ion} \times \frac{k_B T}{N_A q^2} \times \frac{G_m}{C}. \quad (7)$$

Studies on small nonelectrolytes (45,46) show that permeability coefficients in phosphatidylcholine bilayers can be approximated using Eq. 1, with K being the solute partition coefficient between water and hexadecane, and D the solute diffusion coefficient in hexadecane (4×10^{-5} cm^2/s at 25°C (47)). We therefore estimate the apparent partition coefficient of the ions as

$$K_{ion}^{app} = e^{-\Delta G_{trans}^{app}/k_B T} = \frac{P_{ion} \times L}{D}, \quad (8)$$

where L was assigned an approximate value of 40 Å. This formulation is approximate because the ion's free energy varies across the bilayer, and

Eq. 8 provides a lower estimate for the free energy within the bilayer, ΔG_{trans}^{app}. Subsequent modeling of PMF peak height, W_{peak}, is described in the Supporting Material.

RESULTS AND DISCUSSION

Membrane interactions controlling permeation

Equilibrated lipid bilayer systems, with the translocating ion held at the membrane center ($z \approx 0$ Å; Fig. 2), reveal that water molecules and lipid headgroups enter deep inside the membrane core to coordinate the ion. In each case, the ion forms a connection to one interface, with the local deformation being visually similar for all ions. In Fig. 3, *A* and *B*, we compare measurements of bilayer deformations, reporting the number of polar species that enter the bilayer core, which is very similar for all cations (up to ~30 additional water molecules and two to three lipid headgroups may be drawn into the bilayer core). Although somewhat lower (~20 water, ~0.5 headgroups, and ~0.5 K$^+$ counterions) for Cl$^-$, overall the deformations are comparable.

The traditional solubility-diffusion model assumes complete dehydration of ions when they enter the membrane core. In fact, only a small fraction of first-shell hydration
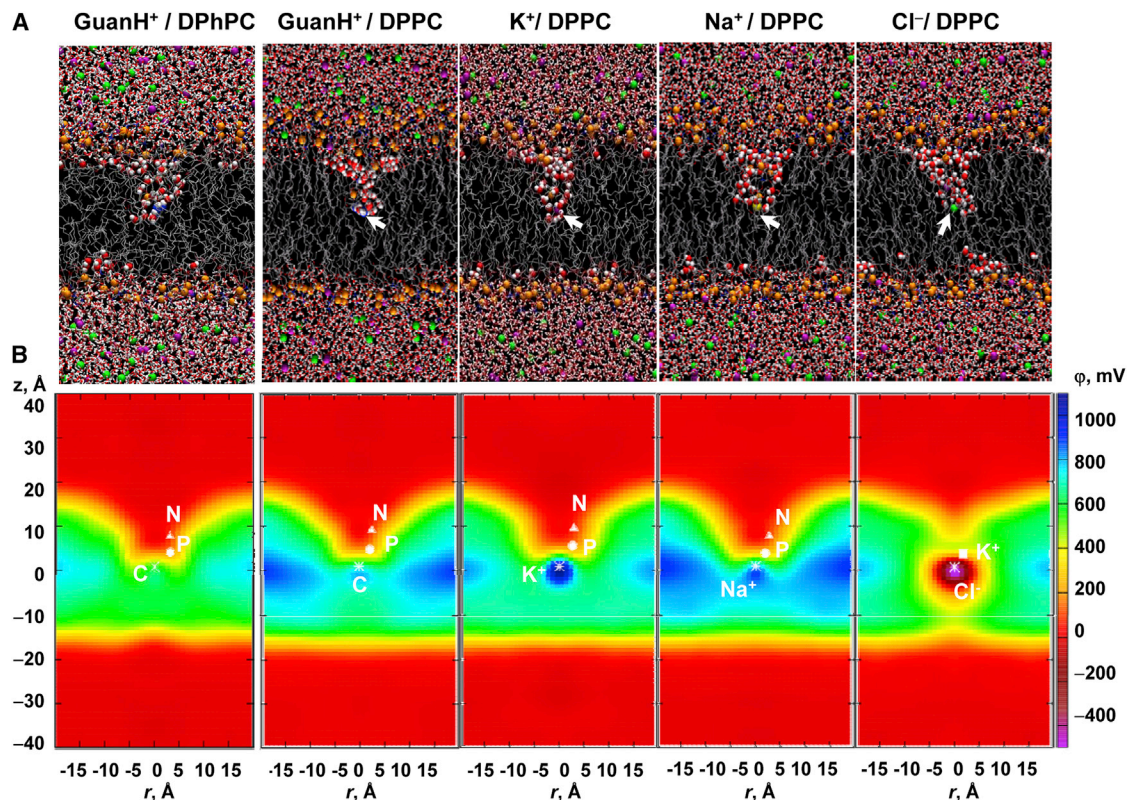

FIGURE 2 (*A*) Snapshots from US simulations for ions crossing DPhPC/DPPC bilayers with the ion positioned near the bilayer center ($z \approx 0$ Å). In all pictures, PC C atoms are gray, N blue, O red, P orange, water red/white, and Na$^+$, K$^+$, and Cl$^-$ ions yellow, purple, and green balls, respectively. Water molecules in the hydrophobic core are shown as balls. (*B*) Electrostatics of the deformable membrane: 2D potential maps (along the *z* axis and at distance *r* from the *z* axis) when the ion is near the center ($z \approx 0$ Å). Average positions are shown for the ion (*asterisk*) (guanidine C for GuanH$^+$) and its closest DPhPC/DPPC P and N atoms (*circle* and *triangle*, respectively), as well as for the K$^+$ counterion (for Cl$^-$; *square*). To see this figure in color, go online.
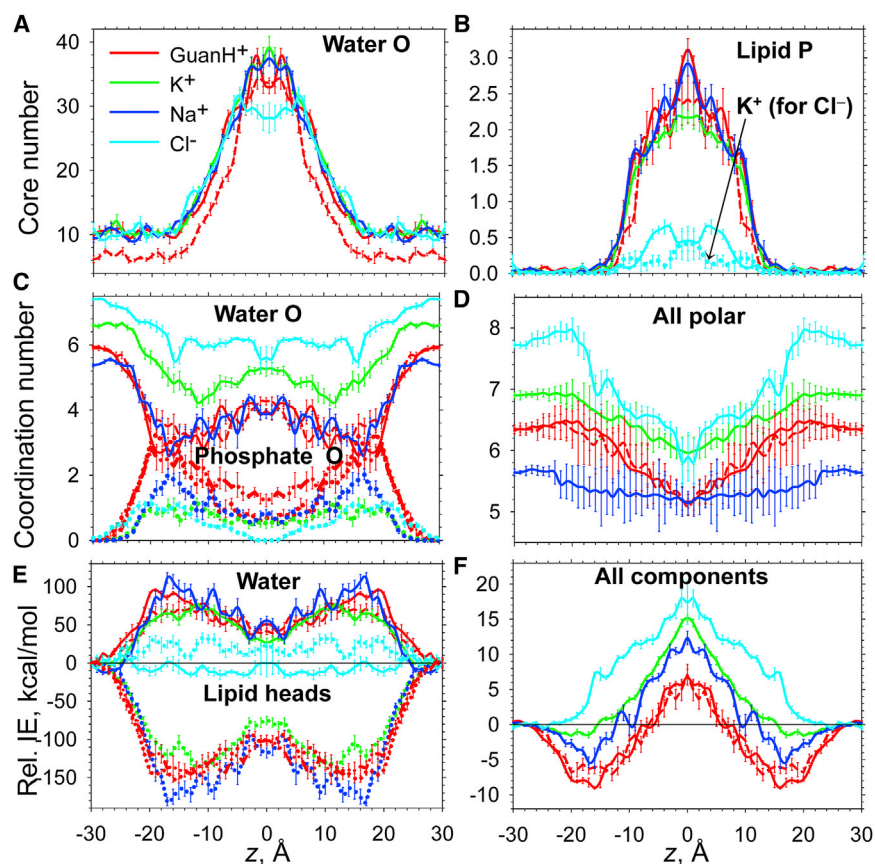
FIGURE 3 (*A* and *B*) Membrane deformations measured by the number of polar species entering the bilayer core ($|z| \leq 13$ Å) for water oxygen (*A*) and lipid P atoms (*B*) (*solid and dashed lines*) and K^+ ions (*dotted line*). (*C* and *D*) Coordination numbers of a translocating ion with water O and lipid phosphate O (for cations; *solid and dashed lines*) or choline N (for Cl^-; *dotted and dash-dotted lines*) (*C*) and for all polar components (*D*). Coordination numbers were obtained as a number of species within interaction distance of the ion (for $GuanH^+ - N_x$ atoms of NH_2 groups; see Fig. S4 *A* for coordination numbers with respect to the central C atom) corresponding to the position of the first minimum on respective radial distribution functions (see Table S1). See Fig. S5 for coordination numbers for other membrane components. (*E* and *F*) Interaction energy contributions for the translocating ion with water (*solid and dashed lines*) and lipid headgroups (*dotted and dash-dotted curves*) (*E*) and with all membrane components, offset to be equal in bulk water (see Fig. S6 for raw data) (*F*). In all graphs, error bars represent the mean ± SEM from block analysis. The results of simulations are shown in red for $GuanH^+$ (DPPC, *solid and dotted lines*; DPhPC, *dashed and dashed-dotted lines*), green for K^+, blue for Na^+, and cyan for Cl^-. To see this figure in color, go online.

is lost, and it is largely compensated for by lipid headgroups (and counterions in the case of Cl^-), as illustrated in Figs. 3 *C* and S5, where the total first-shell solvation by polar components is largely maintained across the membrane (Fig. 3 *D*). Coordination numbers for the different ions vary little inside the membrane core (from ~4.7 for $GuanH^+$ to ~6.0 for K^+). It is this immediate solvation environment, resembling the first hydration shell for each ion in aqueous solutions, that will influence ion permeation energetics and selectivity relative to the solubility-diffusion model.

The ion-induced defect process arises from the large attractive interactions with water and polar lipid moieties (on the order of 100–150 kcal/mol) that drive the membrane deformations. All cations exhibit similar variations in interaction energies with water and lipid headgroups across the bilayer (though these are somewhat larger for Na^+; see Fig. 3 *E* and the absolute values plotted in Fig. S6, *A* and *B*),. The sums of all components (Fig. 3 *F*) are also similar in magnitude (with stronger interactions at the interface for $GuanH^+$ and Na^+ compared to K^+, as suggested previously for the latter two ions (48)). These interactions weaken as a cation moves from the interface into the bilayer core, reflecting partial dehydration and the increased difficulty of deforming the membrane (21,25). This is also evident in Fig. S7, which describes the increased indirect/strain energies and/or entropic costs (due to restricted solvent

motion) associated with membrane deformation. In contrast, the interactions of Cl^- with polar components are almost constant across the membrane, suggesting a slight difference in mechanism. This difference is most evident in comparisons of work decompositions in Figs. S8 and S9, revealing smaller mean forces from lipid components, indicative of reduced bilayer deformation.

The similar ion-membrane interactions among the different cations, and the somewhat different situation experienced by Cl^-, are illustrated by their electrostatic interactions with the bilayer. Fig. 2 *B* shows 2D potential maps for each ion when it is near the bilayer center. The maps reveal deformations that are similar for all cations, where each ion (*asterisk*) is located near the interface between low-potential (*red*) and high-potential (*blue*) regions, experiencing a fairly constant electrostatic force that expels it from the membrane (24). In contrast, Cl^- appears to partially break through the interface. Although reminiscent of the potential seen by a hydrated ion-sized water defect (Fig. S10), it also resembles the ion-induced-defect situation experienced by the cations, thus representing an intermediate process.

The corresponding 1D potential profiles (Fig. S11) confirm that the translocating cations are localized to high-electric field regions, with countercharges (lipid phosphates) also located in regions of significant field, whereas

the choline group of the same coordinating lipid always resides in a region of near-zero field, regardless of the type of cation. This suggests that the leading charge (the permeating cation), and to some extent its immediate countercharge, dominates the ion translocation energetics (24) and is similar for each ion. The anion and its counterion also experience significant fields that will lead to energetics resembling those of the cations. Fig. S12 shows the potential experienced by each translocating ion, φ_{ion}. Remarkably, the variations in electrostatic potential are similarly repulsive for all cations and for the anion Cl^-, in stark contrast to the the prediction of the solubility-diffusion model, where the (highly anion-selective) dipole potential would play an important role (27).

Free-energy profiles for ion permeation

The PMFs for ion permeation across DPPC bilayers are compared in Fig. 4. All ions experience a triangular- or Λ-shaped free-energy profile, where the barriers are similar, varying between 24.1 (for Cl^-) and ~25.8 kcal/mol (for K^+). This similarity of barriers despite the different chemistries, sizes, hydration free energies (varying by >30 kcal/mol; Table S2), and charges of the ions, is astonishing. Using the experimental model bilayer, DPhPC, for comparison, the barrier for GuanH$^+$ is found to be only 0.6 kcal/mol less than that for DPPC.

The lack of thermodynamic ion selectivity stems from the nature of the ion-induced-defect translocation process, determined primarily by the cost of the membrane deforma-
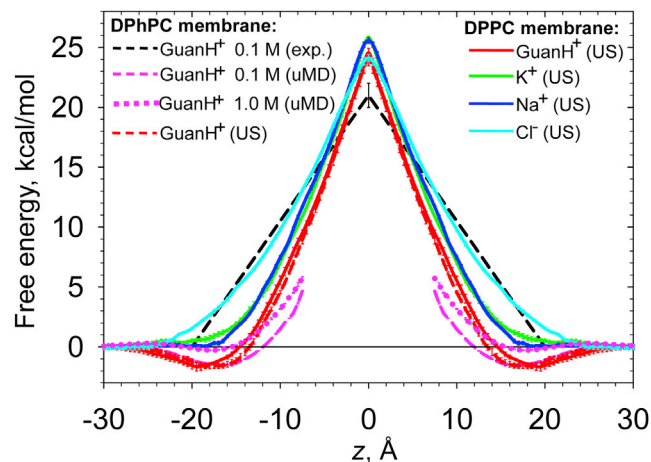

FIGURE 4 Free-energy profiles for ions crossing DPPC and DPhPC bilayers. Error bars are shown as the mean ± 1 SE from block analysis. The results for US MD simulations at 330 K are shown in red for GuanH$^+$ (DPPC, *solid line*; DPhPC, *dashed line*), green for K$^+$, blue for Na$^+$, and cyan for Cl$^-$. The pink dashed and dotted lines were obtained from unbiased microsecond-length equilibrium MD (uMD) simulations at 330 K of a DPhPC membrane with 0.1 and 1.0 M GuanHCl aqueous solution, respectively. An experimental estimate of the free-energy barrier from conductance measurements for DPhPC in 0.1 M GuanHCl solution at 298 K is also shown (*black dashed line*). To see this figure in color, go online.

tions associated with dragging charged and polar components (and their hydrating waters) into the membrane, and not by the dehydration of the ion (which approximately maintains its first solvation shell) or the dipole potential (as the ion does not completely cross the interface and is shielded by its polar environment). In contrast, the solubility-diffusion model would be much more selective and lead to significantly higher barriers, as illustrated in Fig. S13. The selectivity could be better reproduced by a solubility-diffusion process in which ions maintain their first hydration shells (2,3), because the Born energies for partitioning from water to hydrocarbon would be diminished (Table S3 and Fig. S13 B, *dashed curves*). Such a model, however, yields larger variation in energetics and, most importantly, does not capture the lipid bilayer perturbations observed in MD simulations or the correct PMF shape.

The similarity of the free-energy barriers for GuanH$^+$, K$^+$, Na$^+$, and Cl$^-$ indicates that ion dehydration is not a major energetic determinant of transmembrane ion movement. In a related study comparing the roles of arginine and lysine in deforming membranes, we have also computed a PMF for methylammonium that is almost the same as these ions (49). The common free-energy profile suggests similar membrane perturbations for each ion, with their associated costs. GuanH$^+$ is stabilized at the interface by −1.7 kcal/mol (minimum at $|z| \approx 19$ Å), similar to the value determined previously for MGuanH$^+$ (dashed curve in Fig. S4 C), whereas no such minima are present for K$^+$, Na$^+$, and Cl$^-$. The consequence of this interfacial binding of GuanH$^+$ is to shift the PMF downward slightly, but with very similar mean forces acting throughout the membrane. Surprisingly, the barrier for anion permeation is consistent with that for the cations, though the forces experienced by Cl$^-$ are less near the interface, reflecting reduced lipid headgroup penetration (and thus somewhat reduced water penetration) into the bilayer.

One interpretation of this common energetics for all ions is that the path-independent free energy corresponds to the transfer of an ion from water into a deformed membrane that presents an aqueous like environment, with a common energy penalty for the membrane deformation for all ions. This is despite the expectation that the dipole potential would favor anions (by ~10 kcal/mol) (27), which demonstrates that the dipole potential has little impact within the ion-induced-defect process. The lowering of the free-energy barriers for all ions, and the remarkable similarity among different ion types, suggests that ion-induced-defect-driven membrane permeabilities may be consistent with experiments, as we now explore.

Ion diffusion and permeation rates

The one-dimensional (parallel to bilayer normal) diffusion coefficient, D_z, profiles are very similar for all ions (Figs. 5 and S2). All ions experience a rapid drop in D_z as they
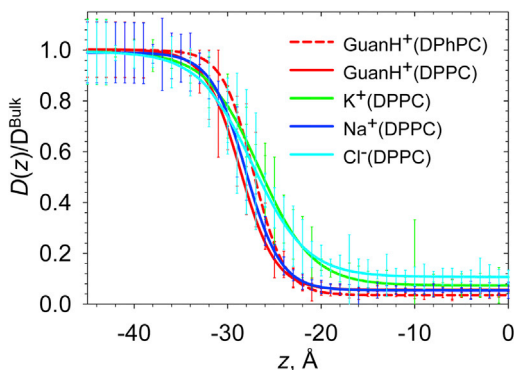
FIGURE 5 Diffusion coefficient profiles, D_z, for ions crossing lipid membranes, relative to bulk water, D^{Bulk} (Table 1) at 330 K. Profiles are shown in red for GuanH$^+$ (DPPC, solid lines; DPhPC, *dashed lines*), green for K$^+$, blue for Na$^+$, and cyan for Cl$^-$. Profiles were obtained by a fourth-order sigmoidal fit to the data, as described in the Supporting Material, and see Fig. S2. To see this figure in color, go online.

approach the interface from the aqueous solution, beginning at ~12 Å from the lipid headgroups, despite the PMF being flat in this region. One must venture far from the membrane interface to encounter truly bulk like water. D_z drops to near minimal values when the ions reach the headgroups, dropping only a little more when entering the bilayer core. We attribute this to the ion always residing at the (deformed) membrane interface, even as it approaches the bilayer center, leading to a sigmoid-type dependence on membrane depth. Relative to bulk values, the diffusion coefficient within the DPPC membrane core drops to as low as ~6% for Na$^+$ and GuanH$^+$, ~7% for K$^+$, and ~11% for Cl$^-$ (Table 1), and results in DPhPC are similar within error (Fig. 5). Such dramatic reductions are not seen for neutral solutes (30,40).

The calculated ion permeability coefficients, $P_{ion,calc}$, (Table 1) are many orders of magnitude less than for water (1.6×10^{-5} cm/s (30)) or other neutral solutes (40). The $P_{ion,calc}$ values vary by only a factor of 8 among the different cations (and at most by a factor of ~23 between Na$^+$ and Cl$^-$), with variations in log P values almost within the uncertainties. These variations can be attributed to modest (~2 kcal/mol) differences in barrier heights and only three-fold variations in diffusion coefficient, as well as changes in the shapes of the free-energy profiles. For GuanH$^+$, $P_{ion,calc}$ across DPhPC approaches twice that for DPPC, but remains within the uncertainty.

Within the errors of the analysis, ion permeation via an ion-induced defect mechanism is remarkably nonselective, as would be expected from the similar PMFs, $W(z)$, and diffusion profiles D_z, which determine the permeability coefficients via Eq. 4. Such analysis makes the assumption that the translocation coordinate, z, captures the rate-limiting step for permeation. Though we have not observed a complete ion translocation even in the constrained equilibrium simulations, which would entail the ion letting go of its connection to one interface and grabbing onto the distant interface—or forming a complete transmembrane defect—the rate-limiting step most likely is associated with traversing the very steep free-energy barrier near the membrane center. Indeed, we have observed interfacial connection transitions within nanoseconds in thinner membranes (29). With fluctuations in bilayer thickness on the order of 4 Å, occurring on the microsecond timescale (see Supporting Material), such transitions should occur relatively quickly in DPPC and DPhPC. Moreover, transitions have also been observed when the ion is moved just beyond the membrane center (20,25), indicating that translocation would be rapid once the steep barrier has been climbed (see Movie S1, described in the Supporting Material). It is important to note that the time for exchange of interfacial connections has been estimated to be on the order of microseconds (50), compared to the timescale of years for ion crossing (see Supporting Material calculations).

Experimental membrane conductance and selectivity

Table 2 summarizes our experimental results for membrane conductances in different bilayers. For the KCl, NaCl, and GuanHCl salts tested, the conductances vary only within an order of magnitude, suggesting that the permeation process is nonselective. The conductances are similar in bilayers formed by ether or ester phospholipids, which have dipole potentials differing by 100–250 mV (28), corresponding to an energy difference of 2.4–6.0 kcal/mol. This suggests that the permeating ions sense little of the membrane dipole potential, consistent with an ion-induced-defect permeation mechanism.

Conductances do not vary much as a function of salt concentration; if anything, they tend to be less in 1.0 M than in 0.1 M salt, which we can understand in terms of loss of

TABLE 1 Calculated all-atom MD simulation results in DPhPC and DPPC bilayers at 330 K

Lipid	Ion	$W_{peak,calc}$ (kcal/mol)	D_{mem}/D_{Bulk} (Å^2/ps)	$P_{ion,calc}$ ($\times 10^{-12}$ cm/s)	log$P_{ion,calc}$ (log(cm/s))	$G_{ion,calc}$ (nS/cm^2)
DPhPC	GuanH$^+$	24.0 ± 0.5	0.011 ± 0.004/0.31 ± 0.03	0.020 ± 0.025	−13.70 ± 0.31	0.068 ± 0.085
DPPC	GuanH$^+$	24.6 ± 0.4	0.017 ± 0.004/0.31 ± 0.03	0.011 ± 0.014	−13.97 ± 0.28	0.037 ± 0.049
	K$^+$	25.8 ± 0.1	0.030 ± 0.012/0.40 ± 0.05	0.0023 ± 0.0022	−14.64 ± 0.21	0.0078 ± 0.0076
	Na$^+$	25.6 ± 0.2	0.017 ± 0.010/0.30 ± 0.04	0.0014 ± 0.0026	−14.85 ± 0.44	0.0048 ± 0.0089
	Cl$^-$	24.1 ± 0.3	0.047 ± 0.012/0.44 ± 0.06	0.033 ± 0.024	−13.49 ± 0.30	0.111 ± 0.081

Results include free-energy barriers, $W_{peak,calc}$; diffusion coefficients D_{mem} at the membrane center, and D_{Bulk} in aqueous solution); permeabilities, P; and contributions to membrane conductance, G_{ion}. All uncertainties are represented as the mean ± 1 SE.

TABLE 2 Experimental conductances for 0.1 or 1.0M GuanHCl, NaCl and KCl in various bilayers at 298K

Lipid	Salt	G (nS/cm^2)
DPhPC/n-decane	GuanHCl 0.1/1 M	6.7 ± 0.7/5.9 ± 1.7
	NaCl 0.1/1 M	3.9 ± 1.3/3.2 ± 0.9
	KCl 0.1 M	5.1 ± 1.2
DphPC/n-decane	GuanHCl 0.1/1 M	1.9 ± 0.2/1.5 ± 0.6
	NaCl 0.1/1 M	1.2 ± 0.5/2.3 ± 0.7
	NaCl^{STS} 0.1/1 M	1.5 ± 0.2/2.1 ± 1.1
DphPC/squalene	GuanHCl 0.1 M	2.4 ± 1.2
	NaCl 0.1 M	2.8 ± 1.0
	KCl 0.1 M	1.8 ± 0.4

Lipid	Salt	V_{rev} (mV)	t_+
DPhPC/n-decane	KCl	−5.2 ± 2.9	0.64 ± 0.09
	GuanHCl	−1.9 ± 2.2	0.55 ± 0.06
DphPC/n-decane	KCl	−10.8 ± 2.9	0.79 ± 0.08
	GuanHCl	4.4 ± 4.0	0.38 ± 0.09

STS denotes reducing conditions in the presence of 4 mM NaS$_2$O$_3$. Reversal potentials and transference numbers for K$^+$ and GuanH$^+$ for DPhPC/n-decane and DphPC/n-decane. Errors are represented as the mean ± standard deviation (SD).

interfacial binding due to screening (Figs. 4 and S14, *dashed and dotted pink lines*; see discussion below). We tested for inadvertent contamination of I$^-$ plus I$_2$ (51) by adding Na$_2$S$_2$O$_3$ to reduce any I$_2$ to I$^-$, eliminating any contribution of polyiodides to the conductance, with no effect (Table 2). Also, similar results were obtained in nominally hydrocarbon-free bilayers formed from DphPC/squalene (Table 2). These measurements could be done only in 0.1 M salt, as squalene bilayers became unstable at higher concentrations. We also examined whether 40 μM phloretin, which produces a large negative change in dipole potential (52), had any effect on DPhPC/n-decane conductance in 0.1 M GuanHCl; it did not (data not shown).

The conductances in NaCl are similar to those reported earlier by Hanai et al. (53): 1.3 or 2.5 nS/cm^2 in egg PC/decane membranes in 0.1 or 1.0 M NaCl. Although we cannot exclude that the experimental results include a contribution from undetected membrane defects (similar to those observed with DphPC/squalene in 1.0 M salt), we conclude that ion movement across lipid bilayers varies little with changes in hydration energy, chemistry, or lipid composition.

To relate the conductances to single-ion permeability coefficients, for comparison with the results from our simulations, we determined reversal potentials and ion transference numbers. Table 2 also summarizes results obtained for DPhPC/n-decane and DphPC/n-decane bilayers (it was not possible to determine the reversal potentials in bilayers containing squalene). Although there is some variation among the different salts and bilayers, there is little cation/anion selectivity, suggesting a common permeation process (and similar energetics for permeation) for the ions studied.

Individual ion permeability coefficients are summarized in Table 3, along with apparent free energies of transfer and approximate peak free energies (using Eqs. 7, 8, and

TABLE 3 Experimental ion permeability coefficients in different bilayers

Lipid	Ion	$P \cdot 10^{-12}$ cm/s	ΔG_{trans}^{app} (kcal/mol)	W_{peak} (kcal/mol)
DPhPC/n-decane	GuanH$^+$ 0.1, 1M	10, 0.9	18, 19	20, 21
	K$^+$ 0.1M	9	18	20
	Cl$^-$ 0.1, 1M	8, 0.7	18, 19	20, 21
DphPC/n-decane	GuanH$^+$ 0.1, 1M	2, 0.2	19, 20	21, 22
	Cl$^-$ 0.1, 1M	3, 0.2	18, 20	20, 22
Bovine brain PS[a]	Na$^+$	0.16		23.5 ± 2.7
	K$^+$	0.91		22.5 ± 3.9
	Cl$^-$	6.5		20.8 ± 0.4
DOPC[b]	K$^+$	3.47		
	Cl$^-$	12100 ± 1400		
Egg lecithin[c]	Na$^+$	0.021 - 0.029		
	Cl$^-$	55		
Ox-brain PS[c]	Na$^+$	0.055		
	Cl$^-$	15		

Results from this work in DPhPC/n-decane and DphPC/n-decane bilayers at 298 K have relative uncertainties of ~50%. Apparent free energies of transfer, ΔG_{trans}^{app}, and estimated peak energy barriers, W_{peak}, for GuanH$^+$, K$^+$ and Cl$^-$ from this study in DPhPC/n-decane and DphPC/n-decane bilayers have uncertainties of ~1 kcal/mol.
[a]Experimental results from Papahadjopoulos et al. (13), for bovine brain PS bilayers at 309 K, with peak values estimated at 300 K.
[b]Experimental results from Paula and co-workers (2,3) for DOPC at 303K.
[c]Experimental results from Hauser et al. (11) at 277 K and pH 5.5 for Cl$^-$.

S6). Within each bilayer, the permeabilities to K$^+$, GuanH$^+$, and Cl$^-$ are similar. As expected from the concentration-independent conductance, the ion permeabilities are ~10-fold less in 1.0 M than in 0.1 M salt. This corresponds to ~1 kcal/mol increase in the estimated energy barriers for ion movement, or a similar reduction in interfacial binding, as suggested by our simulations (Figs. 4 and S14, *dashed and dotted pink lines*).

Our results are consistent with those of previous studies in phospholipid vesicles. In Table 3, we list permeability coefficients for Na$^+$, K$^+$, and Cl$^-$ across bovine phosphatidylserine (PS) membrane (predominantly sn1 -18:0 and sn2 -18: 1-PS, SOPS) (13). Overall, those values are consistent with our results, though they reveal a relatively higher Cl$^-$ permeability, possibly reflecting electroneutral exchange of Cl$^-$ (cf. Toyoshima and Thompson (54)). Papahadjopoulos et al. (13) determined the free-energy barriers of ion permeation to be 20.8 kcal/mol for Cl$^-$, 22.5 kcal/mol for K$^+$, and 23.5 kcal/mol for Na$^+$ at 300 K, reasonably consistent with our estimates for K$^+$, GuanH$^+$, and Cl$^-$. Deamer and colleagues estimated the permeability coefficients for K$^+$ and Cl$^-$ in DOPC membranes to be 3.5 × 10^{-12} cm/s (3) and 1.21 × 10^{-8} cm/s (2), respectively. Their result for K$^+$ is consistent with our result, but that for Cl$^-$ is more than three orders of magnitude higher, presumably reflecting electroneutral Cl$^-$ exchange. Hauser et al. (11) determined the permeability coefficients for Na$^+$ and Cl$^-$ in PC and PS vesicles at 4°C, and their results also are in

general agreement with our results. The permeability coefficient for Cl^-, again, was three orders of magnitude higher than those for cations (again reflecting electroneutral exchange). Overall, our experiments, together with those from other studies, suggest semiquantitative agreement between cation and anion permeabilities and energy barriers (to within a couple of kcal/mol), pointing to a fairly nonselective permeation mechanism.

Comparing MD simulation with experiment

Our MD simulations suggest that all ions tested cross lipid bilayers by an ion-induced-defect mechanism, with similar energetics and diffusion profiles, predicting a fairly nonselective conduction process, consistent with our experimental observations (compare Tables 1 and 3). Both simulations and experiments, however, have uncertainties that complicate quantitative comparisons, and may cause up to three orders of magnitude variation. The use of branched DPhPC in the experiments (as well as the presence of n-decane or squalene) will influence results, though we have shown that a change from DPPC to DPhPC leads to <1 kcal/mol change in the free energy (Fig. 4). We also have shown that a different temperature (330 K vs. 298 K) leads to an ~2 kcal/mol change in the PMF (Fig. S15). It is, however, important that experimental results in different bilayers, both in this study (DPhPC with and without hydrocarbon, and DphPC) and others (DOPC (2,3) and predominantly POPC and SOPS (11,13)) provide general agreement about the magnitude of the permeability coefficients.

The barrier heights obtained in MD simulations are 2–4 kcal/mol higher than estimates deduced from our experimental results (see Fig.4, *black dashed line*, for GuanH$^+$), which may reflect problems with the approximate method used to fit a triangular PMF model to the experiments. The barrier heights deduced from our simulations predict the results of other experiments, to within ~2 kcal/mol (see, e.g., Papahadjopoulos et al. (13), in which bovine brain PS was used). Whereas the statistical uncertainties in both experiments and simulations are on the order of 1 kcal/mol, systematic errors exist due to the choice of experimental technique and lipid type (3), as well as in the model dependence of MD simulation results. One such dependence stems from the lack of explicit electronic polarization of lipid tails, though we have previously shown that the effect is only up to 1 kcal/mol, diminished due to bilayer deformations (24). Small, ~1 kcal/mol force field inaccuracies in ion-headgroup interactions (55), or variations of up to ~3 kcal/mol in PMFs due to different models and force fields (22,23,25) (though within 1–2 kcal/mol when accounting for variation in the strength of interfacial binding), can lead to orders-of-magnitude differences in calculated permeability coefficients. We therefore consider our simulations and experiments to be entirely consistent, though with quantitative agreement remaining a significant challenge.

Microsecond-scale equilibrium simulations reveal ion-induced defects

To explore the ability of an ion to self-induce defects at equilibrium, as suggested by our US simulations, we have carried out microsecond-lengthscale simulations of membranes in bathed in salt solutions. Further, to facilitate comparisons with experiments at different salt concentrations, we compare results from unbiased simulations in 0.1 and 1.0 M GuanHCl solutions, shown as dashed and dotted pink curves in Fig. 4 and visually in Fig. 6 for GuanH$^+$. The results show an ~1 kcal/mol reduction of binding energy due to shielding at higher concentrations, which will impact membrane conductance.

Anions (Cl^-, compared in Fig. S14) are mostly located in the bulk aqueous phase outside the lipid headgroup region (in agreement with previous studies (48)) with a well
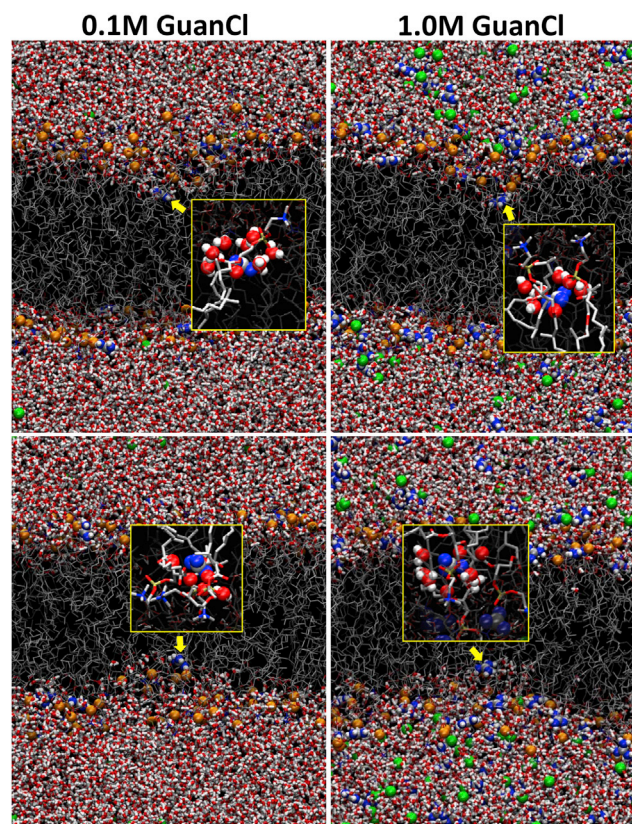

FIGURE 6 Snapshots from ~1.2 μs unbiased MD simulations of DPhPC bilayer in 0.1 M (*left*) or 1.0 M (*right*) GuanHCl aqueous solution. The snapshots show trajectory frames with a GuanH$^+$ ion (*yellow arrow*) closest to the membrane center in upper (top panels) and lower (bottom panels) leaflets. It is located at $z \approx 7.5$ Å (*upper*) or -7.6 Å (*lower*) for 0.1 M GuanHCl simulation and at $z \approx 6.7$ Å (*upper*) or -7.4 Å (*lower*) for 1.0 M GuanHCl simulation. Color scheme is *gray* for C, blue for N, red for O, and orange for P atoms, red/white for water, and green for Cl^- ions. All ions are shown in space-filling presentation. (Insets) Solvation environment of GuanH$^+$ ions, showing water and lipid molecules with their oxygen atoms (*spheres*) in the first solvation shell. To see this figure in color, go online.

defined maximum in density at $\sim|z| = 25.5$ Å in 1.0 M GuanHCl, and a fairly broad distribution (slightly elevated) in the same region ($\sim|z| = 27$ Å) in 0.1 M GuanHCl (Fig. S14 *A*, *green lines*). GuanH$^+$ tends to concentrate in the lipid headgroup region with density maxima at $|z| \sim$ 18 Å or $\sim$17 Å in 1.0 M and 0.1 M GuanHCl solutions, respectively (Fig. S14 *A*, *pink lines*). There are also well-defined minima in the GuanH$^+$ distributions in 1.0 M salt, and corresponding maxima in the Cl$^-$ distribution, indicating the formation of a well defined electric double layer around the membrane.

The corresponding free-energy profiles for Cl$^-$ and GuanH$^+$ are shown in Fig. S14 *B* (*green* and *pink lines*, respectively). Results for 0.1 M GuanHCl compare favorably in the interfacial region to those obtained with US (Figs. 4 and S14 *B*, *red dashed and solid lines*), as do the results for Cl$^-$ across DPPC (Fig. S14 *B*, *cyan line*), despite differences in force field and salt concentration. GuanH$^+$ free-energy profiles have a well-defined minimum of about -0.3 kcal/mol at $|z| \approx 18$ Å in 1.0 M solution and about -1.5 kcal/mol at $|z| \approx 17$ Å in 0.1 M solution. The observed interfacial binding in 0.1 M salt compares favorably to the US estimates of -1.6 ± 0.2 kcal/mol at $|z| \approx 18$ Å in DPhPC and -1.7 ± 0.4 kcal/mol at $|z| \approx 19$ Å in DPPC. The substantial decrease in GuanH$^+$ binding affinity in 1.0 M solution indicates ionic screening and can account for the experimentally observed reduction in ion permeability in this solution (see Table 3 and discussion above). Both GuanH$^+$ and Cl$^-$ profiles climb rapidly after the binding minima (shallow for Cl$^-$; Fig. S14 *B*). Similar but reduced slopes suggest that the unbiased simulations have captured events where ions have moved into the membrane more easily than average, as a result of more favorable local membrane interactions. In much longer timescales, we expect profiles similar to the US results.

We have also determined how deep inside the membrane ions ventured in long unbiased simulations. The deepest Cl$^-$ was on average at $|z| \approx 17.9$ Å and 23.2 Å in 1.0 M and 0.1 M GuanHCl, but approached to as close as $\sim$8.8 Å and $\sim$12.3 Å, respectively, to the membrane center. The deepest GuanH$^+$ (as measured by a central C position) on average ventured to 13.4 Å and 14.5 Å from the membrane center and got as close as $\sim$6.7 Å and $\sim$7.5 Å in 1.0 and 0.1 M GuanHCl simulations, respectively. The ion needs to overcome a free-energy cost of 5–7 kcal/mol to reach this deep into the membrane, explaining why this is a rare event, and why studies of uncatalyzed ion permeation are likely intractable through unbiased simulations alone. The US simulations suggest a barrier of $\sim$9 kcal/mol in this region (Figs. 4 and S14 *B*, *red curves*).The unbiased trajectory snapshots when GuanH$^+$ is deep in the upper and lower leaflets are shown in Fig. 6. There the ion remains coordinated by lipid phosphate, carbonyl oxygens, and water molecules. In both simulations, GuanH$^+$ penetration to 7–8 Å causes substantial membrane deformations, similar to that

observed in US simulations. The spontaneous penetration of the ion leads to ion coordination similar to that seen in biased simulations (on average by approximately five to six water oxygens, one to two lipid phosphates, and one to two carbonyl oxygens at maximum ion penetration depth in the unbiased simulations).

Mechanisms of ion permeation

The ion-induced defect mechanism has been demonstrated in our atomistic US MD simulations for all the cations tested, as well as in separate long unbiased simulations. As discussed above, long unbiased simulations have shown cations venturing into the bilayer core leading to similar deformations and free-energy profiles, demonstrating that ion-induced defects are natural occurrences in membranes. The general agreement between the predicted and observed permeability coefficients, to within a few kcal/mol, together with the almost complete lack of ion selectivity, supports an ion-induced-defect permeation process. In contrast, the alternative direct permeation via a solubility-diffusion mechanism leads to permeability coefficients that differ by many orders of magnitude from experimental observations (1,3,11), as highlighted by the large barriers in Fig. S13 (though these could be improved by allowing partial ion hydration).

For the anion, Cl$^-$, our analysis suggests a mechanism somewhere between ion-induced defect and solubility-diffusion, with a deformed membrane interface and hydrated anion venturing into the membrane (as suggested previously (2,3)), related to the size of the anion and its weaker interactions with lipid headgroups (48). We note that membrane conductance experiments cannot capture the component of conductance originating from electroneutral/carrier-mediated exchange, as seen in radioactive tracer experiments (see, e.g., Toyoshima and Thompson (54) and Khavrutskii et al. (56)). Such a mechanism will lead to enhanced and pH-dependent anion permeability that will dominate the measured permeability for Cl$^-$. Our conductance measurements do, however, better capture the anion translocation process for direct comparison to the cations.

The ion-induced defect mechanism is distinct from the transient pore mechanism, where fluctuations can lead to the formation of water-filled transmembrane pores, exhibiting largely nonselective ion permeation (17) and permeabilities in semiquantitative agreement with experiments (17,57). Such a mechanism is also little dependent on ion hydration energetics, as it is governed primarily by the costs of pore formation (akin to the ion-induced-defect mechanism). We suggest that these processes might occur in tandem, because both originate with membrane deformation involving the displacement of a charge or zwitterion (lipid headgroup (57)) into the bilayer, predicted to have similar energetics (24). Only in thick membranes, with hydrophobic thickness >32 Å (thicker than the usual DPPC or DOPC

models) based on our previous calculations, where the energy costs for bilayer deformations begin to exceed the costs for ion dehydration, will solubility-diffusion permeation of cations come into play (29).

Pinpointing the mechanism of unassisted ion permeation would require quantitative comparison of permeabilities via transient pores and ion-induced defects. This is beyond the current level of accuracy achievable with MD simulations. However, there is much in common between the ion-induced-defect and transmembrane-pore mechanisms. The energetics of moving an ion into the membrane and forming a pore are similar, though it has been suggested that there is a somewhat greater rate of forming localized defects over complete pores (17,58). Moreover, once formed, a transmembrane pore will conduct ions for a duration as short as 5 ns or >150 ns (58). Such multiple permeation events are also expected for single ion-induced defects. It has been shown that a second ion entering an ion-induced defect can move to the bilayer center without additional energetic cost (59), suggesting increased permeation through ion-induced defects.

CONCLUSIONS

We have reported fully atomistic MD simulations, which demonstrate that the physiological cations K^+ and Na^+, the anion Cl^-, and the arginine side chain analog, $GuanH^+$, all deform lipid bilayers to remain hydrated during permeation, in an ion-induced-defect process. Our free-energy calculations have revealed an astonishing lack of effect of ion size, chemistry, and even charge. This lack of selectivity can be rationalized in terms of the membrane deformations that prevent the ion from crossing the membrane interface into the hydrocarbon core. Furthermore, that arginine side chains will experience the same energy penalty for crossing a membrane as any other ion studied is consistent with our understanding of membranes as barriers to charge movement, contrary to recent suggestions that those costs would be smaller (8–10).

The energetics for ion movement across a membrane are different from those predicted by a solubility-diffusion model. The energy barriers emerging from the ion-induced defect model are lower and in reasonable accord with experimental observations. We have shown that, as a result of membrane perturbations, very different hydrophilic ions experience common permeation free-energy and diffusion-coefficient profiles, leading to similar membrane permeabilities, in semiquantitative agreement with experiments. This suggests that direct permeation via an ion-induced defect mechanism could rival transient pore permeation as the dominant permeation process. These results also have significant implications for studies of protein-lipid interactions, including the actions of cell-penetrating peptides, toxins, voltage sensing, and membrane-deforming protein domains.

SUPPORTING MATERIAL

REFERENCES

1. Deamer, D. W., and J. Bramhall. 1986. Permeability of lipid bilayers to water and ionic solutes. *Chem. Phys. Lipids.* 40:167–188.

2. Paula, S., A. G. Volkov, and D. W. Deamer. 1998. Permeation of halide anions through phospholipid bilayers occurs by the solubility-diffusion mechanism. *Biophys. J.* 74:319–327.

3. Paula, S., A. G. Volkov, …, D. W. Deamer. 1996. Permeation of protons, potassium ions, and small polar molecules through phospholipid bilayers as a function of membrane thickness. *Biophys. J.* 70:339–348.

4. Armstrong, C. M., and F. Bezanilla. 1973. Currents related to movement of the gating particles of the sodium channels. *Nature.* 242:459–461.

5. Schmidt, D., Q. X. Jiang, and R. MacKinnon. 2006. Phospholipids and the origin of cationic gating charges in voltage sensors. *Nature.* 444:775–779.

6. Melikov, K., and L. V. Chernomordik. 2005. Arginine-rich cell penetrating peptides: from endosomal uptake to nuclear delivery. *Cell. Mol. Life Sci.* 62:2739–2749.

7. Zasloff, M. 2002. Antimicrobial peptides of multicellular organisms. *Nature.* 415:389–395.

8. Hessa, T., H. Kim, …, G. von Heijne. 2005. Recognition of transmembrane helices by the endoplasmic reticulum translocon. *Nature.* 433:377–381.

9. Jiang, Y., V. Ruta, …, R. MacKinnon. 2003. The principle of gating charge movement in a voltage-dependent K^+ channel. *Nature.* 423:42–48.

10. Moon, C. P., and K. G. Fleming. 2011. Side-chain hydrophobicity scale derived from transmembrane protein folding into lipid bilayers. *Proc. Natl. Acad. Sci. USA.* 108:10174–10177.

11. Hauser, H., D. Oldani, and M. C. Phillips. 1973. Mechanism of ion escape from phosphatidylcholine and phosphatidylserine single bilayer vesicles. *Biochemistry.* 12:4507–4517.

12. Macdonald, R. C. 1976. Energetics of permeation of thin lipid membranes by ions. *Biochim. Biophys. Acta.* 448:193–198.

13. Papahadjopoulos, D., S. Nir, and S. Oki. 1972. Permeability properties of phospholipid membranes: effect of cholesterol and temperature. *Biochim. Biophys. Acta.* 266:561–583.

14. Bangham, A. D., M. M. Standish, and J. C. Watkins. 1965. Diffusion of univalent ions across the lamellae of swollen phospholipids. *J. Mol. Biol.* 13:238–252.

15. Georgallas, A., J. D. Macarthur, …, M. Y. Tse. 1987. The diffusion of small ions through phospholipid bilayers. *J. Chem. Phys.* 86:7218–7226.

16. Glaser, R. W., S. L. Leikin, …, A. I. Sokirko. 1988. Reversible electrical breakdown of lipid bilayers: formation and evolution of pores. *Biochim. Biophys. Acta.* 940:275–287.

17. Gurtovenko, A. A., J. Anwar, and I. Vattulainen. 2010. Defect-mediated trafficking across cell membranes: insights from in silico modeling. *Chem. Rev.* 110:6077–6103.

18. Parsegian, A. 1969. Energy of an ion crossing a low dielectric membrane: solutions to four relevant electrostatic problems. *Nature.* 221:844–846.

19. Wilson, M. A., and A. Pohorille. 1996. Mechanism of unassisted ion transport across membrane bilayers. *J. Am. Chem. Soc.* 118:6580–6587.

20. Tepper, H. L., and G. A. Voth. 2006. Mechanisms of passive ion permeation through lipid bilayers: insights from simulations. *J. Phys. Chem. B.* 110:21327–21337.

21. Dorairaj, S., and T. W. Allen. 2007. On the thermodynamic stability of a charged arginine side chain in a transmembrane helix. *Proc. Natl. Acad. Sci. USA.* 104:4943–4948.

22. MacCallum, J. L., W. F. D. Bennett, and D. P. Tieleman. 2007. Partitioning of amino acid side chains into lipid bilayers: results from computer simulations and comparison to experiment. *J. Gen. Physiol.* 129:371–377.

23. Johansson, A. C. V., and E. Lindahl. 2009. The role of lipid composition for insertion and stabilization of amino acids in membranes. *J. Chem. Phys.* 130:185101.

24. Vorobyov, I. V., B. Bekker, and T. W. Allen. 2010. Electrostatics of deformable lipid membranes. *Biophys. J.* 98:2904–2913.

25. Li, L. B., I. Vorobyov, and T. W. Allen. 2008. Potential of mean force and pKa profile calculation for a lipid membrane-exposed arginine side chain. *J. Phys. Chem. B.* 112:9574–9587.

26. Andersen, O. S., and M. Fuchs. 1975. Potential energy barriers to ion transport within lipid bilayers. Studies with tetraphenylborate. *Biophys. J.* 15:795–830.

27. Flewelling, R. F., and W. L. Hubbell. 1986. The membrane dipole potential in a total membrane potential model. Applications to hydrophobic ion interactions with membranes. *Biophys. J.* 49:541–552.

28. Wang, L. G., P. S. Bose, and F. J. Sigworth. 2006. Using cryo-EM to measure the dipole potential of a lipid membrane. *Proc. Natl. Acad. Sci. USA.* 103:18528–18533.

29. Li, L. B. B., I. Vorobyov, and T. W. Allen. 2012. The role of membrane thickness in charged protein-lipid interactions. *Biochim. Biophys. Acta.* 1818:135–145.

30. Shinoda, W., M. Mikami, …, M. Hato. 2004. Molecular dynamics study on the effects of chain branching on the physical properties of lipid bilayers: 2. Permeability. *J. Phys. Chem. B.* 108:9346–9356.

31. Tristram-Nagle, S., D. J. Kim, …, J. F. Nagle. 2010. Structure and water permeability of fully hydrated diphytanoylPC. *Chem. Phys. Lipids.* 163:630–637.

32. Brooks, B. R., C. L. Brooks, 3rd, …, M. Karplus. 2009. CHARMM: the biomolecular simulation program. *J. Comput. Chem.* 30:1545–1614.

33. Feller, S. E., and A. D. MacKerell. 2000. An improved empirical potential energy function for molecular simulations of phospholipids. *J. Phys. Chem. B.* 104:7510–7515.

34. Jorgensen, W. L., J. Chandrasekhar, …, M. L. Klein. 1983. Comparison of simple potential functions for simulating liquid water. *J. Chem. Phys.* 79:926–935.

35. Sperotto, M. M., and O. G. Mouritsen. 1991. Monte Carlo simulation studies of lipid order parameter profiles near integral membrane proteins. *Biophys. J.* 59:261–270.

36. Torrie, G. M., and J. P. Valleau. 1977. Nonphysical sampling distributions in Monte Carlo free-energy estimation: umbrella sampling. *J. Comput. Phys.* 23:187–199.

37. Kumar, S., J. M. Rosenberg, …, P. A. Kollman. 1992. The weighted histogram analysis method for free-energy calculations on biomolecules. I. The method. *J. Comput. Chem.* 13:1011–1021.

38. Hummer, G. 2005. Position-dependent diffusion coefficients and free energies from Bayesian analysis of equilibrium and replica molecular dynamics simulations. *New J. Phys.* 7:34.

39. Marrink, S.-J., and H. J. C. Berendsen. 1994. Simulation of water transport through a lipid membrane. *J. Phys. Chem.* 98:4155–4168.

40. Bemporad, D., J. W. Essex, and C. Luttmann. 2004. Permeation of small molecules through a lipid bilayer: a computer simulation study. *J. Phys. Chem. B.* 108:4875–4884.

41. Roux, B., and M. Karplus. 1991. Ion transport in a gramicidin-like channel: dynamics and mobility. *J. Phys. Chem.* 95:4856–4868.

42. Redwood, W. R., F. R. Pfeiffer, …, T. E. Thompson. 1971. Physical properties of bilayer membranes formed from a synthetic saturated phospholipid in n-decane. *Biochim. Biophys. Acta.* 233:1–6.

43. MacInnes, D. A. 1961. The Principles of Electrochemistry. Reinhold, New York.

44. Hodgkin, A. L., and B. Katz. 1949. The effect of sodium ions on the electrical activity of giant axon of the squid. *J. Physiol.* 108:37–77.

45. Finkelstein, A. 1987. Water Movement through Lipid Bilayers, Pores, and Plasma Membranes: Theory and Reality. Wiley, New York.

46. Walter, A., and J. Gutknecht. 1986. Permeability of small nonelectrolytes through lipid bilayer membranes. *J. Membr. Biol.* 90:207–217.

47. Schatzberg, P. 1965. Diffusion of water through hydrocarbon liquids. *J. Polym. Sci. C Polym. Symp.* 10:87–92.

48. Gurtovenko, A. A., and I. Vattulainen. 2008. Effect of NaCl and KCl on phosphatidylcholine and phosphatidylethanolamine lipid membranes: insight from atomic-scale simulations for understanding salt-induced effects in the plasma membrane. *J. Phys. Chem. B.* 112:1953–1962.

49. Li, L., I. Vorobyov, and T. W. Allen. 2013. The different interactions of lysine and arginine side chains with lipid membranes. *J. Phys. Chem. B.* 117:11906–11920.

50. Neale, C., C. Madill, …, R. Pomès. 2013. Accelerating convergence in molecular dynamics simulations of solutes in lipid membranes by conducting a random walk along the bilayer normal. *J. Chem. Theory Comput.* 9:3686–3703.

51. Finkelstein, A., and A. Cass. 1968. Permeability and electrical properties of thin lipid membranes. *J. Gen. Physiol.* 52:145–172.

52. Andersen, O. S., A. Finkelstein, …, A. Cass. 1976. Effect of phloretin on the permeability of thin lipid membranes. *J. Gen. Physiol.* 67:749–771.

53. Hanai, T., D. A. Haydon, and J. Taylor. 1965. The variation of capacitance and conductance of bimolecular lipid membranes with area. *J. Theor. Biol.* 9:433–443.

54. Toyoshima, Y., and T. E. Thompson. 1975. Chloride flux in bilayer membranes: chloride permeability in aqueous dispersions of single-walled, bilayer vesicles. *Biochemistry.* 14:1525–1531.

55. Vorobyov, I., L. B. Li, and T. W. Allen. 2008. Assessing atomistic and coarse-grained force fields for protein-lipid interactions: the formidable challenge of an ionizable side chain in a membrane. *J. Phys. Chem. B.* 112:9588–9602.

56. Khavrutskii, I. V., A. A. Gorfe, …, J. A. McCammon. 2009. Free energy for the permeation of Na^+ and Cl^- ions and their ion-pair through a zwitterionic dimyristoyl phosphatidylcholine lipid bilayer by umbrella integration with harmonic Fourier beads. *J. Am. Chem. Soc.* 131:1706–1716.

57. Tieleman, D. P., and S. J. Marrink. 2006. Lipids out of equilibrium: energetics of desorption and pore mediated flip-flop. *J. Am. Chem. Soc.* 128:12462–12467.

58. Gurtovenko, A. A., and J. Anwar. 2007. Ion transport through chemically induced pores in protein-free phospholipid membranes. *J. Phys. Chem. B.* 111:13379–13382.

59. MacCallum, J. L., W. F. D. Bennett, and D. P. Tieleman. 2011. Transfer of arginine into lipid bilayers is nonadditive. *Biophys. J.* 101:110–117.

60. Darden, T., D. York, and L. Pedersen. 1993. Particle mesh Ewald: an N·log(N) method for Ewald sums in large systems. *J. Chem. Phys.* 98:10089–10092.

61. Kucerka, N., S. Tristram-Nagle, and J. F. Nagle. 2006. Closer look at structure of fully hydrated fluid phase DPPC bilayers. *Biophys. J.* 90:L83–L85.

62. Szabo, G., G. Eisenman, and S. Ciani. 1969. The effects of the macrotetralide actin antibiotics on the electrical properties of phospholipid bilayer membranes. *J. Membr. Biol.* 1:346–382.

63. Dror, R. O., R. M. Dirks, …, D. E. Shaw. 2012. Biomolecular simulation: a computational microscope for molecular biology. *Annu. Rev. Biophys.* 41:429–452.

64. Klauda, J. B., R. M. Venable, …, R. W. Pastor. 2010. Update of the CHARMM all-atom additive force field for lipids: validation on six lipid types. *J. Phys. Chem. B.* 114:7830–7843.

65. Allen, T. W., O. S. Andersen, and B. Roux. 2004. Energetics of ion conduction through the gramicidin channel. *Proc. Natl. Acad. Sci. USA.* 101:117–122.

66. Longsworth, L. G. 1954. Temperature dependence of diffusion in aqueous solutions. *J. Phys. Chem.* 58:770–773.

67. Krauss, C. J., and J. W. T. Spinks. 1954. Temperature coefficients for self-diffusion in solution. *Can. J. Chem.* 32:71–78.

68. Nina, M., W. Im, and B. Roux. 1999. Optimized atomic radii for protein continuum electrostatics solvation forces. *Biophys. Chem.* 78:89–96.